Contents list available at IJRED website

International Journal of Renewable Energy Development

Journal homepage: https://ijred.undip.ac.id

Research Article

Numerical Investigation of a New Modified Savonius Wind Turbines

Khalid Mrigua*, Mounia Zemamou, Mohammed Aggour

Laboratory of Electronic Systems, Information Processing, Mechanics and Energy, Faculty of Science, Ibn Tofail University, B.P 133, 14000, Kenitra, Morocco.

Abstract. The classic Savonius semi-circular blade turbine has a relatively low power coefficient. The performance of a Savonius wind turbine depends on its geometrical parameters. Various blade profiles have been developed in the past years to improve the performance of this class of turbine. In this paper, a new blade shapes of Savonius wind turbine is investigated numerically by using the CFD method , by using transient conditions and set k omega turbulence model.The new blade has different concave and convex shape, which is a combination of the conventional and the elliptical blade. A comparative study of three blade profiles, semi-circular, elliptical and the composed blades have been performed. Flow structures around the rotor have also been analyzed. The results show that changing the blade shape has an effect on the performance efficiency of the Savonius turbine. The new modified and the elliptical blade exhibit higher performance compared to the conventional Savonius wind turbine. The new modified Savonius blade and the elliptical blade exhibit an improved performance compared to the conventional model in the order of 20.5% and 18.2% respectively at the tip speed ratio of 0.8.

Keywords: Savonius rotor; Wind energy; Wind turbine; Composed blade, power coefficient.

Received: 15th April 2022; Revised: 25th July 2022; Accepted: 7th August 2022; Available online: 15th August 2022

1. Introduction

The development of technologies based on renewable energy is seen as a solution to meet the growing demand for energy and to limit the impact of global warming. Among the most promising renewable energies sources, wind energy appears as clean source of energy available in the form of kinetic energy from the air.

Based on the axis of rotation, wind turbines are divided mainly among horizontal axis (HAWT) and vertical axis (VAWT) wind turbines (Roy & Saha, 2013a). Savonius rotor was designed by the Finnish Engineer S.J. Savonius in 1931 (Savonius, 1931) with a basic configuration of an "S-shaped" cross-section or a derived configuration composed of two superimposed semi-circular blades. The operating principle is based on the difference of aerodynamic forces. The simple structure of the Savonius rotor allows operation under winds of all directions, resulting in good starting characteristics. The savonius rotor has gained popularity for ventilators and pumping applications, however, due to its low aerodynamic efficiency, the turbine hasn't been used for power generation (Kamoji *et al.*, 2008). Conventional Savonius rotors have an average performance which is characterized by a lower power coefficient. For this reason, the Savonuis rotor has attracted the attention of researchers in order to improve its performance. Many investigations attempt to improve turbine performance by optimizing geometry parameters such as aspect ratio, turbine buckets, end plates. Research into the effect of aspect ratio and overlap ratio on the Savonius rotor shows that the high performance is obtained when the height of the rotor is twice the rotor diameter (Ushiyama & Nagai, 1988), (Fujisawa & Gotoh, 1992) and for an overlap ratio in the range between 0.15-0.25 (Akwa *et al.*, 2012; Jian *et al.*, 2012; Mojola, 1985; Roy *et al.*, 2014) .The influence of the number of blades has also been studied by many researcher (Blackwell et al., 1977),(Mahmoud et al., 2012). These studies have shown that the performance of the wind rotor decreases as the number of blades increases. To optimize the orientation of the air flow around the blades many augmentation technique have been added such as the shields (Morcos *et al.*, 1981, Alexander & Holownia, (1978), deflector (Roy *et al.*, 2014, Youssef *et al.*, 2020), conveyor/deflector (Tartuferi *et al.*, 2015), curtains (Altan & Atılgan, 2010), venting blade (Alom & Saha, 2018), deflector longitudinal (Salleh *et al.*, 2020), V-shaped deflector (Shaughnessy & Probert, 1992), guide vane (El-Askary *et al.*, 2015), straight deflector (Mohamed *et al.*, 2010), they show a considerable improvement in the power of the Savonius wind turbine. The use of a straight deflector resulted in an increase in power coefficient of 27%. The results of developing an optimal shielding configuration show that the peak power coefficient was increased from 0.22 to 0.34. In recent years, severals investigations have been conducted on different blade

* Corresponding author
Email: mriguakhalid@mail.com (K.Mrigua)

https://doi.org/10.14710/ijred.2022.45799
ISSN: 2252-4940/© 2022.The Author(s). Published by CBIORE

shapes to improve the performance of the Savonius rotor. In this context Zemamou *et al* (Zemamou *et al.*, 2020) have introduced a novel blade design based on polynomial Bezier curves and reached a pic value of Cp of about 0.35 at TSR=1.

Zemamou *et al* (Zemamou *et al.*, 2019) have developed a modified design based on elliptical shape with a straight trailing edge the modified design shows a maximum Cp of 0.335, whereas the conventional model indicates the highest Cp of 0.25. the utilization of the elliptical blades in multi-stage systems has been studied by Mrigua *et al.* (Mrigua *et al.*, 2020). It is found that the two stages rotor has a higher power coefficient than the single and three stage rotors. Kamoji. (Kamoji *et al.*, 2009a) has carried out an investigation on the Bach-profile rotor without the central shaft. Their result shows that the maximum Cp obtained is 0.21 at Re= 1.510^5. The disadvantage of a conventional Savonius turbine is the low power and torque coefficient, which is a significant obstacle to the application of Savonius wind turbines (Abdelaziz *et al.*, 2022), (He, 2017).

In order to surmount this problem, some studies have already been conducted, optimizing the geometric parameters of the blades (Sheldahl *et al.*, 1978) (Kacprzak et al., 2013) (Akwa *et al.*, 2012) (Afroz *et al.,* 2012), (Sobczak, 2018), and (Chen *et al.*, 2022). This results in a slight increase in the efficiency of the rotor.

Other researchers have studied and analyzed some additional devices or obstacles (Fig.1.d and 1c), to improve the performance of Savonius wind turbines, which leads to a significant increase. However, this modification will increase the complexity of the rotor construction and potentially reduce the starting capacity

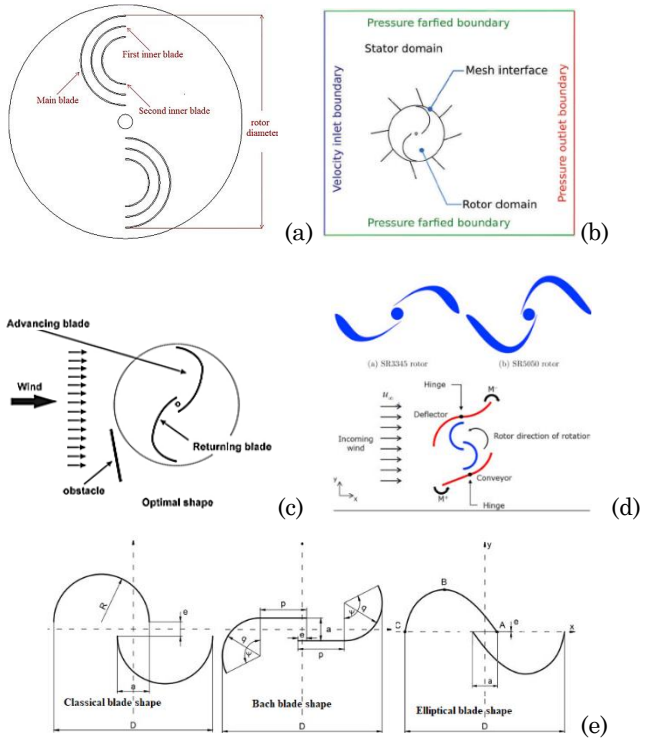

Fig. 1 Various design of savonius rotor, (a) semi-circular with two internal blades(Al-Ghriybah *et al.*, 2021), (b) modified Savonius (Kalluvila & Sreejith, 2018), (c) obstacle shielding returning blade (Mohamed *et al.*, 2011), (d) SR3345 airfoil SR5050 airfoil and Conveyor-deflector curtain (Tartuferi *et al.*, 2015) (e) Semi-circular, Elliptique and Bach shapes.

From an aerodynamic point of view, the wind blowing on the Savonius rotor blades creates a lift force and a drag force. The problem of minimizing the performance of the wind turbine is related to the negative drag force produced by the returning blade that pushes the rotor in the opposite direction of rotation, which requires a change in profile. The developed design in this paper has a concave part of the with straight part and another part with a higher curvature than the semicircular profile which causes the increase of the drag on the concave surface, has an impact on the overall net torque of the turbine. In addition, the straight part of the blades also acts positively and accelerates the rotor moment.

2. Methodology

The objective of this paper is to present a new composed design of blade based on different combination of conventional and elliptical blades. The new blade has a different concave and convex shape, which is a combination of the conventional blade representing the convex side and the elliptical blade representing the concave side. The rotation mechanism of the Savonius turbine is mainly affected by the increase in concave drag, which affects the overall net torque of the turbine.

The new blade is flatter and thicker than the conventional blade. As the elliptical profile has an almost straight part and another part with a higher curvature than the conventional profile, they mainly cause a difference in pressure drag.

The conventional, elliptical and the new developed Savonius wind turbine are depicted in figure below (Fig. 2). To assess the performance of the investigated designs, the CFD modeling technique is used. The shear stress transport (SST) k-ω turbulence model is employed to simulate the flow field around these turbines. The published experimental results by A. Sanusi (Sanusi et al., 2016) are used to validate the performed model. A comparative study of three blade profiles, semi-circular, elliptical and composed blades have been performed. Finally, this paper provides an analysis of the flow field including velocity and, pressure distribution

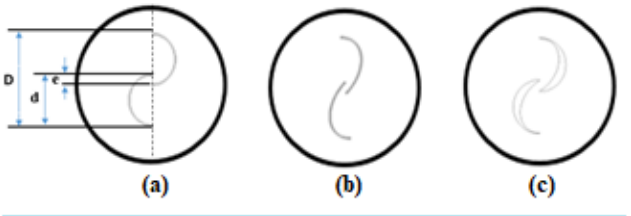

Fig.2 (a) Conventional Savonius rotor, (b) Elliptic rotor, (c) Composed rotor.

Table 1
Geometrical parameters of Savonius rotors.

Rotor diameter D	Chor of blade d	Overlap ratio (e/d)
0.514 m	0.2855 m	0.2

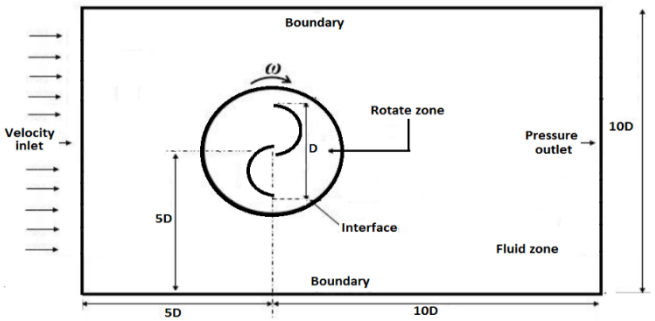

Fig. 3 Sketch of the computational domain

2.1 Computational domain

In the present study, the Fluent software was used to model the flow around the Savonius rotors. The two-dimensional computational domain and the boundary conditions are shown in Figure 3.

The computational domain has two parts separated by a sliding interface: a rotate domain (circular zone) and a fix domain (rectangular zone), the dimension of the computational domain is 10D×15D. The Savonius rotors, is located at the center of the rotate domain, placed at a distance 5D from the top and bottom sides of the rectangular domain, and at a 5D distance upwind, where the condition of inlet velocity was assigned.

2.2. Mathematical Model

This paragraph discusses the mathematical equations that are used in the modeling. These equations combine the different flow parameters. For an incompressible flow, the equations governing the conservation of the mass and the momentum are given respectively by:

$$\frac{\partial \rho}{\partial t} + \frac{\partial}{\partial x_i}(\rho u_i) = 0 \quad (1)$$

$$\frac{\partial}{\partial x_i}(u_i) + \frac{\partial}{\partial x_j}(u_i u_j) = -\frac{1}{\rho}\frac{\partial p}{\partial x_i} + \nu \frac{\partial^2 u_i}{\partial x_j \partial x_j} \quad (2)$$

Where $\nu = \frac{\mu}{\rho}$, u_i, p, x_i and t are respectively, the kinematic viscosity, the flow velocity, pressure, and spatial and temporal coordinates. The numerical solution uses the notion of average variables. It is therefore necessary to transform the NS equations into averaged equations according to the Reynolds decomposition. Reynolds' method consists of decomposing each physical variable into an average and a fluctuating value:

$$u = \bar{u} + u' \quad (3)$$

The equations governing the conservation of the mass and momentum are (averaged by Reynolds' procedure) given respectively by:

- Continuity equation:

$$\frac{\partial}{\partial x_i}(\overline{u_i}) = 0 \quad (4)$$

- Momentum equation:

$$\frac{\partial}{\partial x_i}(\overline{u_i}) + \overline{u_j}\frac{\partial}{\partial x_j}(\overline{u_i}) = -\frac{1}{\rho}\frac{\partial \bar{p}}{\partial x_i} + \nu \frac{\partial^2 \overline{u_i}}{\partial x_j \partial x_j} + \frac{\partial}{\partial x_j}\left(-\rho \overline{u_i' u_j'}\right) \quad (5)$$

Where $-\rho \overline{u_i' u_j'}$ is the Reynolds stress tensor (Celik, 1999). This requires additional modelling to close the RANS equations which leads to the creation of different turbulence models such as the S-A model, the k-Ɛ model and the k-ω model. The Boussinesq hypothesis is used to solve the Reynolds stresses. Equation is expressed as follow:

$$-\rho \overline{u_i' u_j'} = \mu_t \left(\frac{\partial \bar{u}_i}{\partial x_j} + \frac{\partial \bar{u}_j}{\partial x_i}\right) - \frac{2}{3}\left(\rho k + \mu_t \frac{\partial u_K}{\partial x_k}\right)\delta_{ij} \quad (6)$$

Where $k = \frac{1}{2}\overline{u_i' u_i'}$, and $\mu_t \approx \rho\sqrt{k}.l$ represent respectively the Turbulence kinetic energy and the eddy viscosity. Here l is the turbulent length scale.

2.3. Turbulence Model

In this study, the SST k-ω turbulence model (Menter, 1994) has been utilized, due to its efficiency and better prediction (Ferdoues *et al.*, 2017). The SST k-ω is a combination between two models, the turbulence model k-ε and the model of turbulence k-ω (Song *et al.*, 2015; Mishra *et al.*, 2019). The SST k- ω model has two partial equations where 'k' is the turbulence kinetic energy and ω mention to a specific dissipation.

- Turbulence kinetic energy:

$$\frac{\partial k}{\partial t} + \overline{u_j}\frac{\partial k}{\partial x_j} = \frac{\partial}{\partial x_i}\left[(v + \sigma_k v_t)\frac{\partial k}{\partial x_j}\right] + P_k - \beta^* \omega k \quad (7)$$

- Specific dissipation rate

$$\frac{\partial \omega}{\partial t} + \overline{u_j}\frac{\partial \omega}{\partial x_j} = \frac{\partial}{\partial x_i}\left[(v + \sigma_\omega v_t)\frac{\partial \omega}{\partial x_j}\right] + p_k \frac{\gamma}{\nu_t} - \beta\omega^2 + 2(1 - F_1)\sigma_{\omega^2}\frac{1}{\omega}\frac{\partial k}{\partial x_j}\frac{\partial \omega}{\partial x_j} \quad (8)$$

2.4. Performance parameter

Considering the solution of conservation equations and the chosen turbulence model, the torque of rotor (T) can be calculated by integrating the force difference resulting from the shear and the pressure on the rotor as shown below (Nasef *et al.*, 2013):

$$M = \sum_i \left(F_{i,\text{pressure}} + F_{i,\text{shear}}\right) \cdot d \quad (9)$$

$$M = \sum_i \left((\lfloor P_i - P_{\text{ref}} \rfloor A_i) + [-\tau_i A_i].\right)_{\text{concave}} \cdot d - \sum_i \left((\lfloor P_i - P_{ref} \rfloor A_i) + [-\tau_i A_i].\right)_{\text{convex.}} d \quad (10)$$

where Fi pressure and Fi shear are the pressure and shear forces vectors acting on the face area vector Ai respectively and d is a local torque arm vector from the rotation axis, about which the moment is taken. where p and τ are the pressure and shear stress, respectively. The Coefficient of Torque C_T, Coefficient of Power C_P and Coefficient of Static Torque are given respectively from the following equations (Mahmud *et al.*, 2018).

$$C_T = \frac{T}{T_W} = \frac{4T}{\rho \times A \times d \times V^2} \quad (11)$$

$$C_P = \frac{P}{P_w} = \frac{2T \times \Omega}{\rho A V^3} = C_T \times TSR \quad (12)$$

$$C_{T_S} = \frac{4T_S}{\rho \times A \times d \times V^2} \quad (13)$$

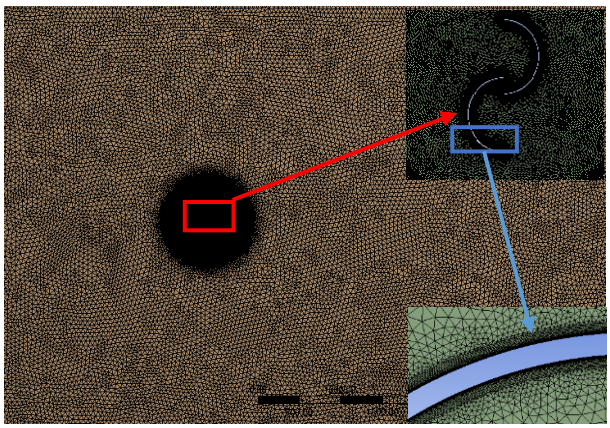

Fig. 4 Mesh for basic and modified configuration rotating domain.

Static torque is the net torque of the rotor in the Static state. Which is principally responsible for the starting capacity of the rotor (Roy & Saha, 2013b).

2.5. Meshing and boundary condition

The domain of computational is discretized using unstructured hybrid grids. The mesh must be fine enough to resolve with precision the physics of the flow, in particular at the level of the boundary layer in the vicinity of the rotor surface. For this reason, the inflation meshing technique is applied to the rotors wall, by creating layers of fine mesh in the direction normal to a wall. The first layer thickness takes the value of 5.10^{-5} m the growth rate of 1.2 as shown in Figure 4, this value was calculated using the equation 7.

$$y^+ = \frac{\rho u_t dy}{\mu} \quad (14)$$

The frictional velocity u_t is calculated from the following equation:

$$u_t = \left(\frac{\tau_\omega}{\rho}\right) \quad (15)$$

Table 2
Parameters and Boundary condition.

Boundary condition	Parameter	value
Inlet	U	6.2 m.s^{-1}
Outlet pressure	P	0 Pascal
Angular velocity	ω	4.8-28.9 rad. s^{-1}
Blade walls	No slip condition	-
Turbulence intensity	I	5%
Pressure velocity coupling	SIMPLE	-
Special discretization	Second order upwind	-
Number of complet revolutions	N	10
Convergence criteria	Residual Monitors	10^{-5}

Where τ_ω represents wall shear stress, dy is the distance of first cell from rotors wall and μ= 1,811.10^{-5} Ns.m^{-2} is the dynamic viscosity. Figure 5 shows the y+ variations for all Savonius rotors at rotation angle 90°. In order to capture the flow properties in the vicinity of the blade, a mean y+ value of less than 1 can be observed.

The SIMPLE (Semi-Implicit Method for Pressure Linked Equations) pressure-velocity coupling method was used in all simulations for all the equations, a second order wind spatial discretization algorithm has been used, and a Least Squares Cell Based algorithm has been used for the gradients. Table 2 reports the boundary condition parameters and solver configuration.

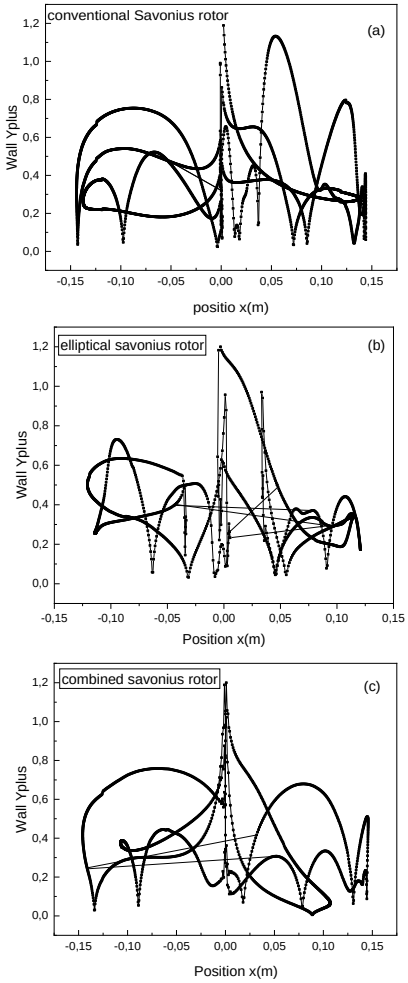

Fig.5 Y+ around the blades of the Savonius rotor at θ = 90°, (a) Convectional blade (b) Elliptical blade (c) Composed blade

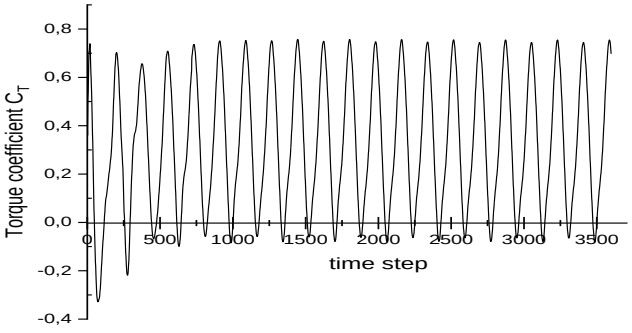

Fig. 6 Variation of torque on the rotor with Flow time at TSR 0.8

Figure 6 shows the C_T of the Conventional Savonius rotor in 10 rotation periods are plotted against the rotation angle. It can be seen that after the 3 period, the variation in C_T almost follows a periodic variation, and is therefore averaged to give a more precise value.

3. Results and discussion

3.1. Grid-independent test

Numerical simulation is carried out over five completed rotations of the turbine. The maximum number of iterations per time step fixed at 50. Absolute criteria are used to monitor the convergence of the solution with a value of 10^{-5} (Table 2). The mesh is one of the most important parameters of the simulation to achieve high accuracy and avoid lack of convergence. The grid-independent test has been carried out by varying the grids between 50,000 and 300,000, the averages Cp of the grids is shown in Figure 7. The simulation results show that there is no significant change in the coefficient of torque beyond 130000 elements

3.2. Validation of the numerical methodology

The simulation results of the flow around conventional wind turbine Savonius with two blades, using the SST $k-\omega$ turbulence model were compared with the experimental results from (Sanusi *et al*., 2016) to evaluate the precision the current numerical methodology. The variation of the torque coefficient, of both experimental and numerical approach for different tip speed ratios, are shown in Figure 8.

The maximum error value between the experimental and numerical data about 6.25% at λ=0.2. The pattern variation of both curves show a similar behavior. The computational results have a good accord with the experiment test. As a result, it is suitable to perform the numerical method in order to foresee the performance of Savonius rotors.

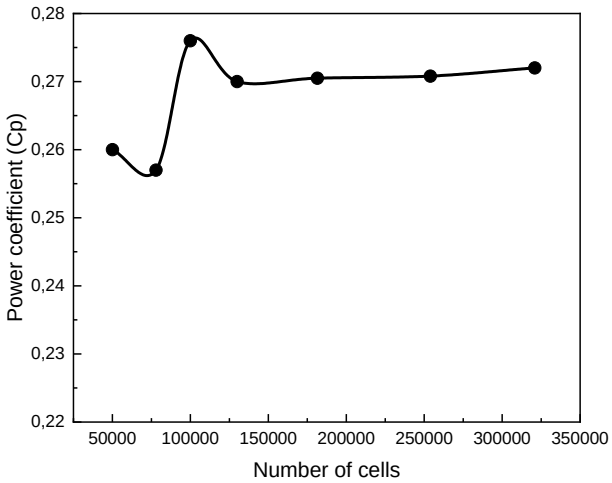

Fig. 7 Power coefficient variation with number of cells

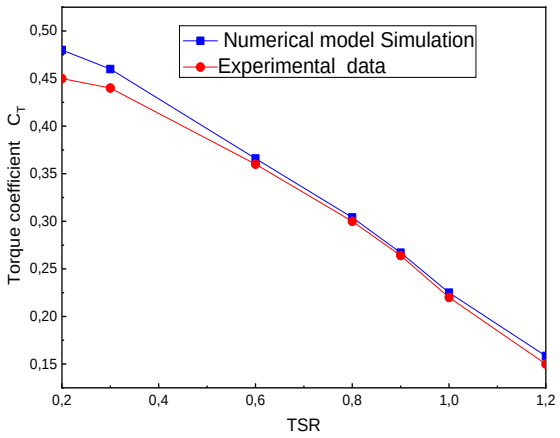

Fig. 8 Numerical and Experimental data (Sanusi et al., 2016) of torque coefficient CT

3.3. Comparison of the geometries conception.

In the present investigation, 2D unsteady simulations is conducted on the semi- circular bladed, elliptical bladed and composed bladed under identical conditions. Figure 9 shows the variations in the power coefficient C_P and the torque coefficient C_T for the three profiles with the Tip Speed Ratio.

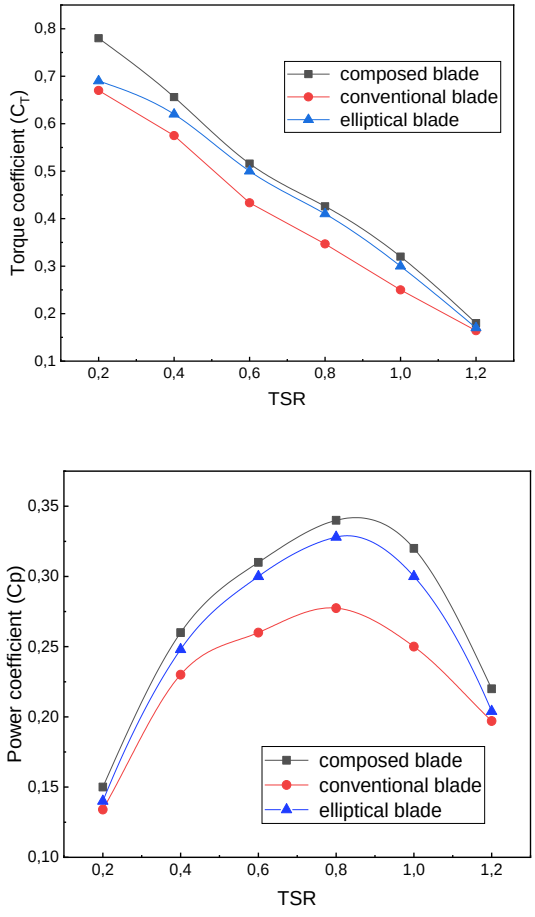

Fig. 9 Comparison of the average torque and power coefficient at different TSRs.

From the analysis, it can be noticed that the rotor speed decreases with the application of load, and therefore the variation of C_T decreases when TSR increases, (Figure 9). The composed profile has higher power coefficients over the tested range of TSR compared to elliptical and conventional profiles. The composed blade shows a CP peak of 0.34 at TSR=0.80, whereas at the similar TSR, the CP peak is 0.33 and 0.27 for the elliptical and the semicircular profiles, respectively. The simulation thus exhibits an improvement of CP in the composed profile compared to the semicircular profiles by 20.5%. The coefficient of power decreases for all blade models beyond TSR = 0.8. It is believed that the power coefficients of elliptical and conventional profiles are reduced due to the formation of vortices downstream of the return blades. The coefficient of torque as a function of time at tip speed ratio 0.8 is shown in Figure 10. It can be noted that the values of torque coefficient the composed-blade are greater over the conventional-blade rotor. Concentrate on the last revolution of simulation, a comparison of the moment coefficient versus rotor angle θ for the two rotor types is shown in Figure 11.

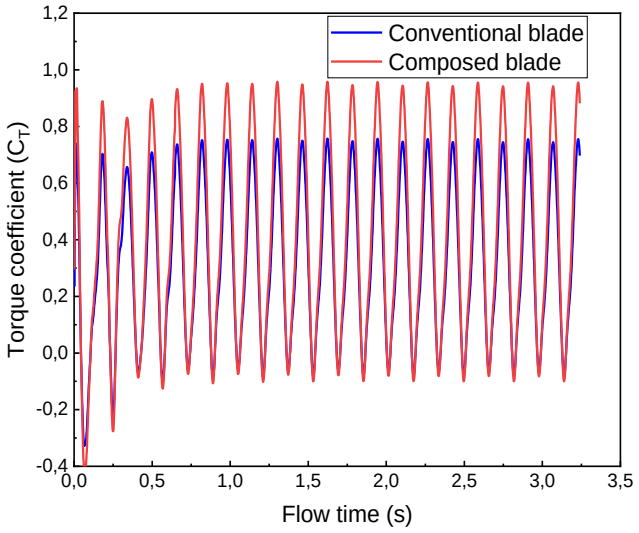

Fig. 10 Torque Coefficient versus flow time.

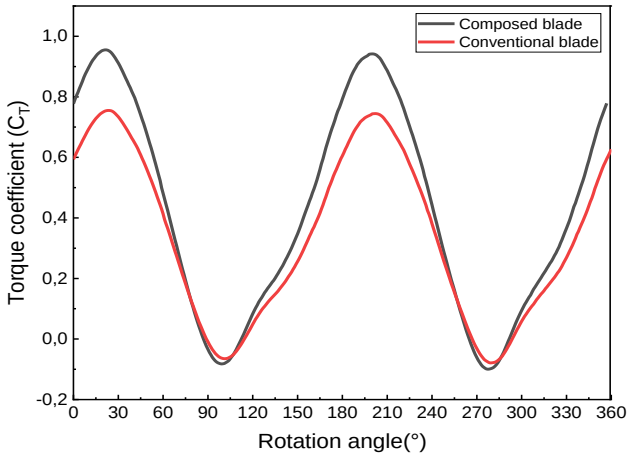

Fig. 11 Comparison of instantaneous torque coefficient versus rotor angle for conventional and composed blades.

The curves of the instantaneous torque coefficient of the two rotors show a similar trend within one rotation period. The instantaneous torque coefficient is covered by two cycles in one revolution. The torque values of the composed blade rotor are generally higher than the conventional blade rotor, except for rotor angles between [75°-105°] and [255°-285°]. The maximum value of torque for the composed blade rotor occurs at rotor angles of 22° and 202°, and it is about 20.5% higher compared to the conventional blade rotor at rotor angles of 25° and 205°. The ability to accept wind from various directions is similar for the combination blade rotor and the conventional blade rotor. The composed blade rotor exhibits an increase in the torque coefficient resulting in an improvement in the power coefficient.

3.4. Pressure and velocity contours

The contours of the pressure of three rotor profiles are shown in Figure 12. It is clearly observed that the pressure in the composed profile is of the order of 20-40 N/m^2, whears in the other profiles the pressure found to be lesser. On the concave side of the returning blade, the pressure for the composed profile is higher than the other ones. The pressure on the concave face of the blade can contribute to the increase of the positive torque, while the convex face has the possibility to reduce the rotor torque. In addition, the higher pressure zone on the convex side of the returning blade of the composed profile is lower than the other ones, the resulting torque is therefore higher in the composed profile. In addition, the effect of overlapping flows is more prominent for composed blades, which reduces the negative torque (Kacprzak *et al.*, 2013). whereas, the effect of overlapping flow and a better pressure field on the concave side of the returning blade is more substantial, in the composed blade as compared to other ones. The pressure contours for composed blade are similar to Saeed *et al.*, (2019).

The amplitude of the velocity near the surface of the advancing profile is around 1.5 to 4 m.s^{-1}, 2.5 to 4 m.s^{-1} and 3.5 to 5 m.s^{-1} for semicircular, elliptic and composed blades respectively. The magnitude of velocity in the convex side of the returning blade is lower in the composed blade than the others ones. It is observed that the flow gets accelerated near the tip of the blades, the high velocity zone is relatively closer to the surface of the composed blade than that of the others profiles, and it can also be seen that the tip losses are greater in the semi-circular and elliptic blades than in the composed blade. An overlapping jet, is formed on the concave face of the advancing blade and reaches the retuning blade. The overlapping is found to be more prominent in the composed blade 5-6.5 m/s than the semicircular blade 3-4.5 m/s and elliptic blade 3.5-5 m/s. The increase in speed in this area suggests that the negative contribution of the returning blade to the overall torque is considerably reduced. The formation of wake on the concave side of returning blade of composed profile is found to be smaller than the semicircular and elliptical profiles

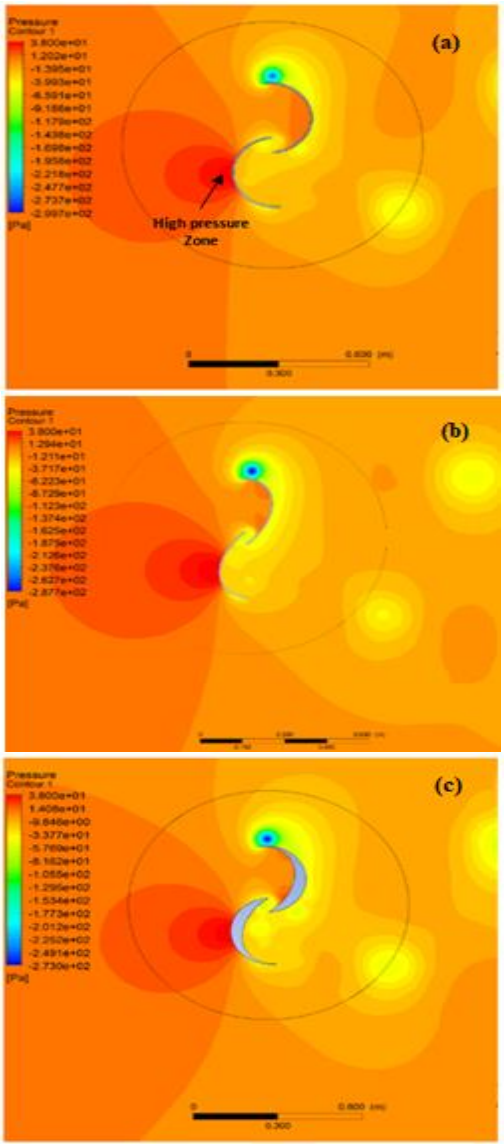

Fig. 12 Pressure contours (Pascal) of (a) conventional, (b) elliptical and (c) composed profiles at TSR = 0.8.

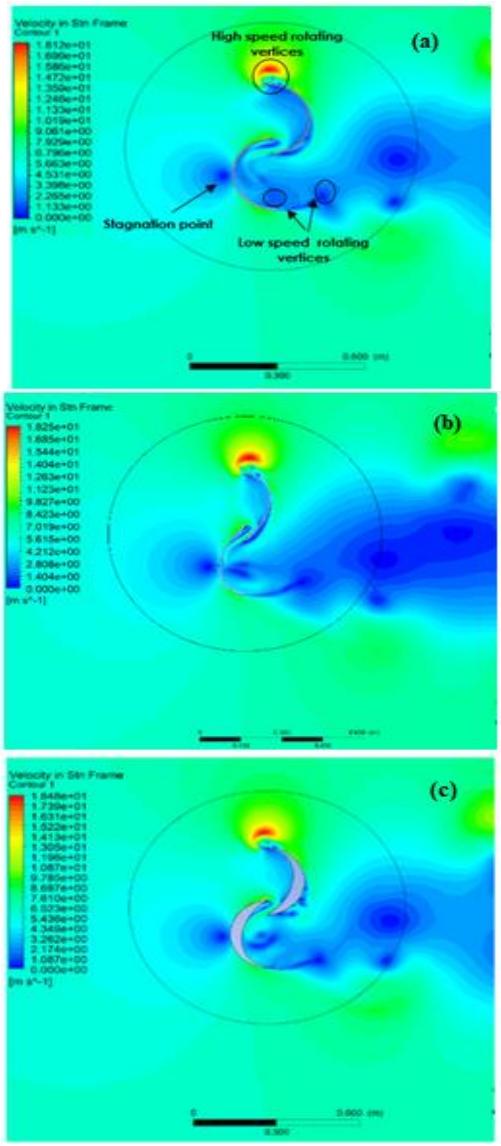

Fig. 13 Velocity of (a) conventional, (b) elliptical and (c) composed profiles TSR = 0.8

3.5. Effect of number Reynolds

The study of a vertical axis wind turbine subjected to operating conditions in the presence o f wind is very complex, because the wind has an instantaneous variation in speed and direction. The wind velocity is adjusted corresponding to a given Reynolds number $R_e = \frac{UD}{v}$. Both conventional and composed wind turbines are tested at different Reynolds numbers corresponding to wind speeds of 3.2 m.s^{-1} , 4.2 m.s^{-1} , 6.2 m.s^{-1} and 7.2 m.s^{-1} . Figure 14 shows the variation of power coefficient at different Reynolds numbers. These curves have similar trends for the power coefficients of all rotors. The maximum Cp values were found for all rotors at a TSR of 0.8. The power coefficient increase as a function of the Reynolds number. (Kamoji *et al.*, 2009b). The maximum coefficient of power increases with the increase in the Reynolds number. This increase in Cpmax with increased Reynolds number has also been noted by Sheldahl (Sheldahl *et al.*, 1978) for conventional Savonius rotors. Reynolds number plays a very major role in the aerodynamic performance.

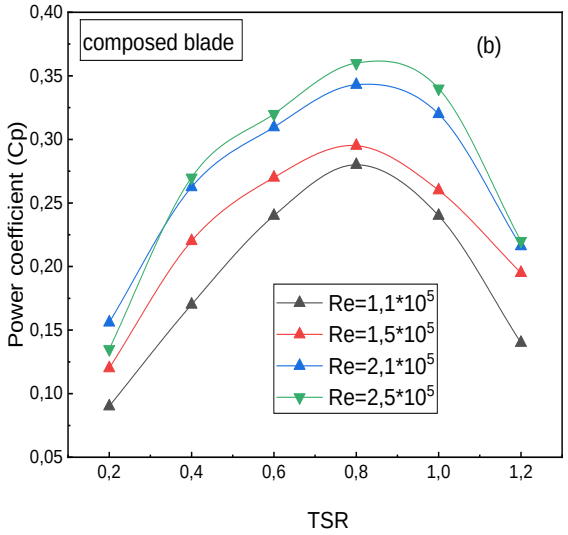

Fig.14 Evolution of the power coefficient with the TSR, for (a) conventional blade, and (b) composed blade at different number Reynolds.

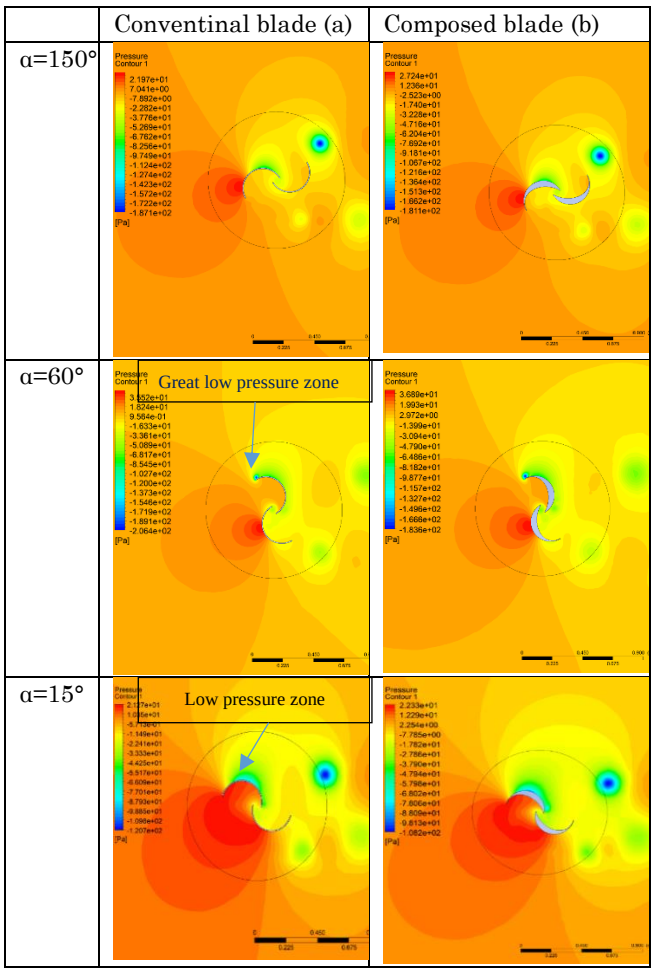

Fig. 15 The pressure contours of (a) the semicircular and (b) the composed profiles

3.6. Effect of Rotor angle

Figure 15 shows the pressure contours of the composed and the semicircular profiles as a function of the rotor angle. At 15°, on the concave side of both blades seems to have high pressure. the pressure distribution for all rotors tested is almost the same, but the suction area and pressure amplitude for composed blades is larger than that of the conventional blades. Consequently, in the rotor with alpha 15° blades, the pressure difference for composed blade causes additional force, and in results, an improvement in performance. It is clear from the contours, that there is a strong fluctuation in pressures resulting in high turbulence behind the conventional blade rotor.

At α=60° the first one being a low-pressure zone near the tip at 60° and the second one being a high-pressure zone bon the mid of the convex surface of the blade at 240°. The returning blade of conventional profiles, a high-pressure zone appears on the convex side, and a low-pressure zone appears on the concave side compared to composed profiles. The pressure differential provides a high torque that prevents the turbine from rotating. At 150°, a great low-pressure vortex leaves the top of the advancing blade. It is observed that such pressure difference is higher in the composed profile than the semicircular profile. This results in a higher Cp in the composed profile.

3.7. Self-starting

Finally, in order to verify the ability of the improved system to self-start, the static torque coefficient was calculated for both conventional and composed blades at different rotor angles. Figures 16 gives the variation of the static torque coefficient for both rotors as a function of the rotor angle.

Table 3
The values of the maximum power coefficients corresponding to investigations concerning various blade profiles

Authors	Methodology	Rotor profile	Performance
Al-Ghriybah *et al.*, (2021)	2D k-ε/ realizable	Semi-circular	0.16
		semi-circular with two internal blades.	0.177
Kacprzak *et al.*, (2013)	*2D k-ω SST* model	Semi-circular	0.153
		Elliptique	0.17
		Bach	0.18
Antar & Elkhoury, (2019)	2D *k-ω SST* model	Semi-circular	0.232
Mari *et al.*, (2017)	2D Spalart–Allmaras	spline	0.2477
Ferrari *et al.*, (2017)	2D *k-ω SST* model	Semi-circular	0.266
Tartuferi *et al.*, (2015)	v^2-f and RSM	SR3345*airfoil*	0.25
	models(Conveyor/deflector)	SR5050 *airfoil*	0.22
		Semi-circular	0.27
Emmanuel & Jun, (2011)	2d RNG k-ε	Semi-circular	0.27
Mohamed *et al.*, (2011)	w2D realizable *k-ϵ* model	Optimal shape	0.30
Banerjee *et al.*, (2014)	2D *k-ω SST* model	Semi-circular	0.28
		Elliptique	0.31
Kalluvila & Sreejith, (2018)	k-epsilon model (Guide blades)	modified Savonius	0.32
Present study	2D *k-ω SST* model	Semi-circular	0.27
		Pales composé	0.34

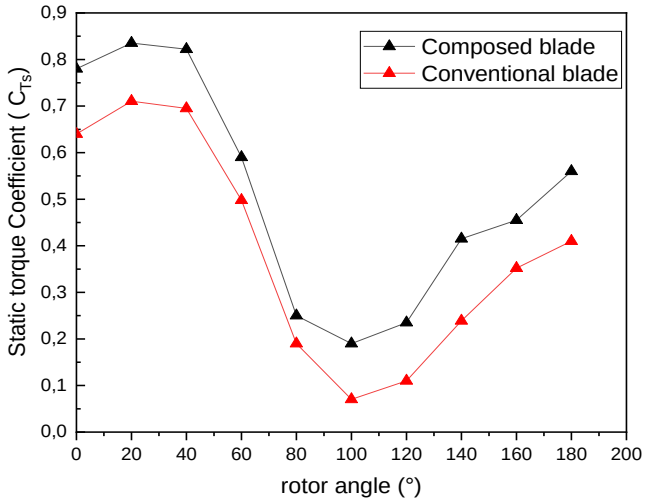

Fig. 16 Coefficient of static torque C_{Ts} as a function of rotor angle θ for both composed and conventional blades.

It can be seen that the conventional and composed blades show a similar evolution of the static torque coefficient characteristics. The conventional Savonius rotor is a self-starting rotor, this feature is retained for the composed blade rotor. To highlight the results achieved, a comparison with the findings of other investigators involved in the development of the Savonius wind turbine blades is presented in the table below. It can be observed that the power coefficient found in this study is higher than the power coefficients derived from previous investigations.

4. Conclusion

The Savonius rotor is a small-scale wind power system, but it suffering from low efficiency. Therefore, the main objective of this study is to develop an improved design, which produces higher performance. In this work, we present a new form of Savonius wind turbine blade combining two different sides. The convex part has the semicircular shape of the conventional blade. The concave part is elliptical. The aerodynamic performances of these Savonius rotors are studied using CFD. 2D unsteady simulations using the SST k-ω turbulence model are conducted for the composed, Elliptical and Semicircular profiles at a wind speed of 6.2 $m.s^{-1}$. Moreover, to confirm the accuracy of the computational results, a validation of the simulation results against experimental data is performed. The results of the simulation around the conventional blade of the Savonius rotor show good agreement with experimental data. The composed blade wind turbine has a Cpmax =0.34, whereas that of the conventional SSWT is 0.27, this means that a performance improvement of 20.5% is achieved with the composed blades over the conventional blade profile at the tip speed ratio of 0.8. Regarding the Reynolds number effect on the performance of the savonius rotor, the results confirm that the composed blade has a better performance than the conventional blade at different Reynolds numbers. Thus, the new modified Savonius wind turbines have significantly better self-start than the conventional design. In this study we have developed a compound blade to be used as a new model of the savonius rotor, for future studies we could consider using this model in multistage rotors to increase the power output.

Acknowledgments

Authors would like to thank the late Mr. Toumi. for contributing

References

Abdelaziz, K. R., Nawar, M. A., Ramadan, A., Attai, Y. A., & Mohamed, M. H. (2022). Performance improvement of a Savonius turbine by using auxiliary blades. *Energy*, 244, 122575. https://doi.org/10.1016/j.energy.2021.122575

Afroz, Z., Islam, M. Q., & Ali, M. (2012). Aerodynamic studies on multi-bladed S-shaped vane type rotor. 2nd *International Conference on the Developments in Renewable Energy Technology (ICDRET 2012)*, 1-3.

Akwa, J. V., da Silva Júnior, G. A., & Petry, A. P. (2012). Discussion on the verification of the overlap ratio influence on performance coefficients of a Savonius wind rotor using computational fluid dynamics. *Renewable energy*, 38(1), 141-149. https://doi.org/10.1016/j.renene.2011.07.013.

Alexander, A. J., & Holownia, B. P. (1978). Wind tunnel tests on a Savonius rotor. *Journal of Wind Engineering and Industrial Aerodynamics*, 3(4), 343-351. https://doi.org/10.1016/0167-6105(78)90037-5

Al-Ghriybah, M., Zulkafli, M. F., Didane, D. H., & Mohd, S. (2021). The effect of spacing between inner blades on the performance of the Savonius wind turbine. *Sustainable Energy Technologies and Assessments*, 43, 100988. https://doi.org/10.1016/j.seta.2020.100988

Alom, N., & Saha, U. K. (2018). Performance evaluation of vent-augmented elliptical-bladed savonius rotors by numerical simulation and wind tunnel experiments. *Energy,* 152, 277-290. https://doi.org/10.1016/j.energy.2018.03.136

Altan, B. D., & Atılgan, M. (2010). The use of a curtain design to increase the performance level of a Savonius wind rotors. *Renewable Energy*, 35(4), 821-829. https://doi.org/10.1016/j.renene.2009.08.025

Antar, E., & Elkhoury, M. (2019). Parametric sizing optimization process of a casing for a Savonius Vertical Axis Wind Turbine. *Renewable Energy*, 136, 127-138. https://doi.org/10.1016/j.renene.2018.12.092

Banerjee, A., Roy, S., Mukherjee, P., & Saha, U. K. (2014). Unsteady flow analysis around an elliptic-bladed Savonius-style wind turbine. *Gas Turbine India Conference*, 49644, V001T05A001. https://doi.org/10.1115/GTINDIA2014-8141

Blackwell, B. F., Feltz, L. V., & Sheldahl, R. E. (1977). Wind tunnel performance data for two-and three-bucket Savonius rotors. Sandia Laboratories Albuquerque, New Mexico.

Celik, I. B. (1999). Introductory turbulence modeling. Virginia, Western Virginia University.

Chen, Y., Guo, P., Zhang, D., Chai, K., Zhao, C., & Li, J. (2022). Power improvement of a cluster of three Savonius wind turbines using the variable-speed control method. *Renewable Energy*. https://doi.org/10.1016/j.renene.2022.05.062

El-Askary, W. A., Nasef, M. H., Abdel-Hamid, A. A., & Gad, H. E. (2015). Harvesting wind energy for improving performance of Savonius rotor. *Journal of Wind Engineering and Industrial Aerodynamics*, 139, 8-15. https://doi.org/10.1016/j.jweia.2015.01.003

Emmanuel, B., & Jun, W. (2011). Numerical study of a six-bladed Savonius wind turbine. *Journal of Solar Energy Engineering*, 133(4). https://doi.org/10.1115/1.4004549

Ferdoues, M. S., Ebrahimi, S., & Vijayaraghavan, K. (2017). Multi-objective optimization of the design and operating point of a new external axis wind turbine. *Energy*, 125, 643-653. https://doi.org/10.1016/j.energy.2017.01.070

Ferrari, G., Federici, D., Schito, P., Inzoli, F., & Mereu, R. (2017). CFD study of Savonius wind turbine : 3D model validation

and parametric analysis. *Renewable energy*, 105, 722-734. https://doi.org/10.1016/j.renene.2016.12.077

Fujisawa, N., & Gotoh, F. (1992). Pressure measurements and flow visualization study of a Savonius rotor. *Journal of Wind Engineering and Industrial Aerodynamics*, 39(1-3), 51-60. https://doi.org/10.1016/0167-6105(92)90532-F

He, D. (2017). Aerodynamic shape optimization of Savonius wind turbines. HKUST Thesis. https://doi.org/10.14711/thesis-991012551768203412

Jian, C., Kumbernuss, J., Linhua, Z., Lin, L., & Hongxing, Y. (2012). Influence of phase-shift and overlap ratio on Savonius wind turbine's performance. *Journal of solar energy engineering,* 134(1). https://doi.org/10.1115/1.4004980

Kacprzak, K., Liskiewicz, G., & Sobczak, K. (2013). Numerical investigation of conventional and modified Savonius wind turbines. *Renewable energy*, 60, 578-585. https://doi.org/10.1016/j.renene.2013.06.009

Kalluvila, J. B., & Sreejith, B. (2018). Numerical and experimental study on a modified Savonius rotor with guide blades. *International journal of green energy,* 15(12), 744-757. https://doi.org/10.1080/15435075.2018.1529574

Kamoji, M. A., Kedare, S. B., & Prabhu, S. V. (2008). Experimental investigations on single stage, two stage and three stage conventional Savonius rotor. *International journal of energy research*, 32(10), 877-895. https://doi.org/10.1002/er.1399

Kamoji, M. A., Kedare, S. B., & Prabhu, S. V. (2009a). Experimental investigations on single stage modified Savonius rotor. *Applied Energy,* 86(7-8), 1064-1073. https://doi.org/10.1016/j.apenergy.2008.09.019

Kamoji, M. A., Kedare, S. B., & Prabhu, S. V. (2009b). Performance tests on helical Savonius rotors. *Renewable Energy,* 34(3), 521-529. https://doi.org/10.1016/j.renene.2008.06.002

Mahmoud, N. H., El-Haroun, A. A., Wahba, E., & Nasef, M. H. (2012). An experimental study on improvement of Savonius rotor performance. *Alexandria Engineering Journal*, 51(1), 19-25. https://doi.org/10.1016/j.aej.2012.07.003

Mahmud, M. S., Reza, K. N., & Rahman, M. Z. (2018). Performance Study of a Small-Scale Water Current Turbine.

Mari, M., Venturini, M., & Beyene, A. (2017). A Novel Geometry for Vertical Axis Wind Turbines Based on the Savonius Concept. *Journal of Energy Resources Technology*, 139(6). https://doi.org/10.1115/1.4036964

Menter, F. R. (1994). Two-equation eddy-viscosity turbulence models for engineering applications. *AIAA journal*, 32(8), 1598-1605. https://doi.org/10.2514/3.12149

Mishra, A., Kumar, G., & De, A. (2019). Prediction of separation induced transition on thick airfoil using non-linear URANS based turbulence model. *Journal of Mechanical Science and Technology,* 33(5), 2169-2180. https://doi.org/10.1007/s12206-019-0419-6

Mohamed, M. H., Janiga, G., Pap, E., & Thévenin, D. (2010). Optimization of Savonius turbines using an obstacle shielding the returning blade. *Renewable Energy,* 35(11), 2618-2626. https://doi.org/10.1016/j.renene.2010.04.007

Mohamed, M. H., Janiga, G., Pap, E., & Thévenin, D. (2011). Optimal blade shape of a modified Savonius turbine using an obstacle shielding the returning blade. *Energy Conversion and Management,* 52(1), 236-242. https://doi.org/10.1016/j.enconman.2010.06.070

Mojola, O. O. (1985). On the aerodynamic design of the Savonius windmill rotor. *Journal of Wind Engineering and Industrial Aerodynamics*, 21(2), 223-231. https://doi.org/10.1016/0167-6105(85)90005-4

Morcos, S. M., Khalafallah, M. G., & Heikel, H. A. (1981). The effect of shielding on the aerodynamic performance of Savonius wind turbines. *16th Intersociety Energy Conversion Engineering Conference*, 2037-2040.

Mrigua, K., Toumi, A., Zemamou, M., Ouhmmou, B., Lahlou, Y., & Aggour, M. (2020). CFD Investigation of A New Elliptical-Bladed Multistage Savonius Rotors. *International Journal of Renewable Energy Development*, 9(3). https://doi.org/10.14710/ijred.2020.30286

Nasef, M. H., El-Askary, W. A., Abdel-Hamid, A. A., & Gad, H. E. (2013). Evaluation of Savonius rotor performance : Static and dynamic studies. *Journal of Wind Engineering and Industrial Aerodynamics,* 123, 1-11. https://doi.org/10.1016/j.jweia.2013.09.009

Roy, S., Mukherjee, P., & Saha, U. K. (2014). Aerodynamic performance evaluation of a novel Savonius-style wind turbine under an oriented jet. *ASME 2014 Gas Turbine India Conference*. https://doi.org/10.1115/GTINDIA2014-8152

Roy, S., & Saha, U. K. (2013a). Computational study to assess the influence of overlap ratio on static torque characteristics of a vertical axis wind turbine. *Procedia Engineering*, 51, 694-702. https://doi.org/10.1016/j.proeng.2013.01.099

Roy, S., & Saha, U. K. (2013b). Review of experimental investigations into the design, performance and optimization of the Savonius rotor. *Proceedings of the Institution of Mechanical Engineers, Part A: Journal of Power and Energy*, 227(4), 528-542. https://doi.org/10.1177/0957650913480992

Saeed, H. A. H., Elmekawy, A. M. N., & Kassab, S. Z. (2019). Numerical study of improving Savonius turbine power coefficient by various blade shapes. *Alexandria Engineering Journal,* 58(2), 429-441. https://doi.org/10.1016/j.aej.2019.03.005

Salleh, M. B., Kamaruddin, N. M., & Mohamed-Kassim, Z. (2020). The effects of deflector longitudinal position and height on the power performance of a conventional savonius turbine. *Energy Conversion and Management*, 226, 113584. https://doi.org/10.1016/j.enconman.2020.113584

Sanusi, A., Soeparman, S., Wahyudi, S., & Yuliati, L. (2016a). Experimental study of combined blade savonius wind turbine. *International Journal of Renewable Energy Research (IJRER),* 6(2), 614-619. https://doi.org/10.20508/ijrer.v6i2.3455.g6826

Savonius, S. J. (1931). The S-rotor and its applications. *Mechanical engineering*, 53(5), 333-338.

Shaughnessy, B. M., & Probert, S. D. (1992). Partially-blocked Savonius rotor. *Applied Energy,* 43(4), 239-249. https://doi.org/10.1016/0306-2619(92)90024-6

Sheldahl, R. E., Blackwell, B. F., & Feltz, L. V. (1978a). Wind tunnel performance data for two-and three-bucket Savonius rotors. *Journal of Energy*, 2(3), 160-164. https://doi.org/10.2514/3.47966

Sobczak, K. (2018). Numerical investigations of an influence of the aspect ratio on the Savonius rotor performance. *Journal of Physics: Conference Series*, 1101(1), 012034. https://doi.org/10.1088/1742-6596/1101/1/012034

Song, C., Zheng, Y., Zhao, Z., Zhang, Y., Li, C., & Jiang, H. (2015). Investigation of meshing strategies and turbulence models of computational fluid dynamics simulations of vertical axis wind turbines. *Journal of Renewable and Sustainable Energy,* 7(3), 033111. https://doi.org/10.1063/1.4921578

Tartuferi, M., D'Alessandro, V., Montelpare, S., & Ricci, R. (2015). Enhancement of Savonius wind rotor aerodynamic performance: A computational study of new blade shapes and curtain systems. *Energy*, 79, 371-384. https://doi.org/10.1016/j.energy.2014.11.023

Ushiyama, I., & Nagai, H. (1988). Optimum design configurations and performance of Savonius rotors. *Wind Engineering*, 59-75.

Youssef, K. M., El Kholy, A. M., Hamed, A. M., Mahmoud, N. A., El Baz, A. M., & Mohamed, T. A. (2020). An innovative augmentation technique of savonius wind turbine performance. *Wind Engineering*, 44(1), 93-112. https://doi.org/10.1177/0309524X19849860

Zemamou, M., Toumi, A., Mrigua, K., & Aggour, M. (2019). Modified Design of Savonius Wind Turbine Blade for Performance Improvement. *International Journal of Innovative Technology and Exploring Engineering (IJITEE),* 9(1). https://doi.org/10.35940/ijitee.A4202.119119

Zemamou, M., Toumi, A., Mrigua, K., Lahlou, Y., & Aggour, M. (2020). A novel blade design for Savonius wind turbine based on polynomial bezier curves for aerodynamic performance enhancement. *International Journal of Green Energy,*

17(11), 652-665.
https://doi.org/10.1080/15435075.2020.1779077